Degrees of polarization of the two strongest $5f \rightarrow 3d$ lines following electron-impact excitation and dielectronic recombination processes of Cu-like to Se-like gold ions

Z. W. Wu, C. Z. Dong,* and J. Jiang

Key Laboratory of Atomic and Molecular Physics & Functional Materials of Gansu Province, College of Physics and Electronic Engineering, Northwest Normal University, Lanzhou 730070, People's Republic of China

(Received 20 May 2012; published 22 August 2012)

Cross sections for electron-impact excitation and capture to individual magnetic sublevels of Cu-like to Se-like gold ions have been calculated by using a fully relativistic distorted-wave (RDW) method. These magnetic cross sections have further been used to obtain the degrees of linear polarization for the first two strongest $5f \rightarrow 3d$ radiative lines. A detailed comparison has been made between polarizations of these lines from the electron-impact excitation process and those of the same lines but from the dielectronic recombination process. It is found that for a Cu-like gold ion the polarization in the electron-impact excitation process increases sharply before starting to decrease at higher incident electron energies, and it reaches the maximum at around twice the threshold energy. The situations for other gold ions are very similar. However, as for the dielectronic recombination process, the polarization changes among a very large range with different gold ions. Therefore, the obvious differences between the polarizations from different formation processes can be employed in diagnosing the formation mechanism of the corresponding lines.

DOI: 10.1103/PhysRevA.86.022712 PACS number(s): 34.80.Dp

I. INTRODUCTION

High-temperature plasmas extensively exist in tokomaks [1–3], vacuum sparks [4], astrophysical objects [5], Z pinches [6–9], solar plasmas [10,11], and laser-produced plasmas [12–15]. Important parameters must be correctly predicted to know these plasmas, such as charge state distribution (CSD), energy balance, radiation levels, energy deposition rate, the linear polarization of emission lines, and so on. In the indirect laser drive of inertial confinement fusion (ICF), gold is used as a work material of particular interest in a hohlraum [12,16]. A laser beam heats the inside of a gold hohlraum-producing plasma which emits intense x-ray radiations. The x ray drives the capsule implosion and influences the resulting fusion yield. So many works have been devoted to, for example, x-ray emission spectra, radiative opacity, CSD, and the electron-impact excitation process of gold ions or plasmas. Gold x-ray spectra in ICF relevant spectral regions have been previously studied by Kiyokawa *et al.* [17]. They recorded the $5f \rightarrow 3d$ and $6f \rightarrow 3d$ line groups of Ni-like to Ga-like gold ions. However, those line groups were misidentified as being composed of the $6d_{3/2} \rightarrow 3p_{3/2}$ and $6d_{3/2} \rightarrow 3p_{1/2}$ transitions. In later laser-produced plasma experiments, Bauche-Arnoult *et al.* [18] remeasured and correctly identified these line groups. Honda *et al.* [19] theoretically studied the x-ray spectra of highly charged nonlocal thermodynamical equilibrium (NLTE) gold plasma and calculated part of the excitation energies and oscillator strengths of the $4f \rightarrow 3d$ transitions for Ni-like to Ga-like ions. Zhang *et al.* [20,21] theoretically studied the emission spectra of laser-produced plasmas. Yi *et al.* [22] calculated the wavelength, transition probability, and oscillator strength for laser-produced gold plasmas. May *et al.* [23] presented a systematic study on the emissions from Ni-like to Kr-like gold ions by using the Livermore electron beam ion traps EBIT-I and EBIT-II; they recorded the emissions from $n = 4 \rightarrow 3$, $5 \rightarrow 3$, $6 \rightarrow 3$, and $7 \rightarrow 3$ x-ray transitions from Ni-like to Kr-like gold ions between 1500 and 5000 eV by employing both a photometrically calibrated x-ray microcalorimeter and an x-ray crystal spectrometer. The line emission from the gold ions was observed in steady state at a density of $\sim 10^{12}$ cm^{-3}. The plasmas with this density have fewer active atomic physics processes and are easier to be modeled than the laser-produced plasma experiments. Träbert *et al.* [24] used these plasmas to identify and to measure the photon energies of the $n = 4 \rightarrow 4$ extreme ultraviolet transitions between 30 and 60 Å from Cu-like to Kr-like gold ions. Zeng [25] studied x-ray emission spectra of Ni-like gold ions under coronal plasma condition by using the flexible atomic code (FAC). In an experiment with the NOVA laser, Foord *et al.* [26] inferred the average charge state $\langle q \rangle$ value of gold plasma from the $5f \rightarrow 3d$ lines of the Ni-like to Kr-like ions. In this experiment, a gold microdot buried in Be foil was heated by laser to steady-state conditions with $T_e = 2.2$ keV and $n_e = 6 \times 10^{20}$ cm^{-3}. The $\langle q \rangle$ value of +49.3 was inferred by comparing the recorded spectrum with modeling from the Hebrew University Lawrence Livermore atomic code (HULLAC) [27]. Glenzer *et al.* [28] also measured the $5f \rightarrow 3d$ lines emitted from fusion hohlraum plasma with $T_e = 2.6$ keV, $n_e = 1.4 \times 10^{21}$ cm^{-3}, and $T_{\rm rad} = 210$ eV and inferred the $\langle q \rangle$ value of $+52(\pm 1)$. Foord *et al.* and Glenzer *et al.* found reasonable agreement between the observed $\langle q \rangle$ value and theoretical prediction from the plasma modeling code RIGEL [29]. Wong *et al.* [30] experimentally measured the CSD of highly charged gold plasma by using the spectral emissions. The measured average ionization state was 46.8 ± 0.75 in the gold plasma with a Maxwell-Boltzmann temperature of 2.5 keV and an electron density of $\sim 10^{12}$ cm^{-3}. For the experimental case mentioned above, Peyrusse *et al.* [31] performed calculations of the charge state distribution involving all ions from Au^{40+} to Au^{51+}; the corresponding ionization state was 46.4, in good agreement with the experimental result 46.8 ± 0.75. Heeter

*Corresponding author: dongcz@nwnu.edu.cn

et al. [32] carried out a series of benchmark measurements of the ionization balance of highly charged NLTE gold plasmas at electron densities near 10^{21} cm^{-3} and electron temperatures spanning the range 0.8–2.4 keV. They analyzed time- and space-resolved M-shell gold emission spectra by using the collisional-radiative model and found average ionization states $\langle q \rangle$ ranging from 42 to 50. May *et al*. [33] performed a systematic study of gold CSD from low-density and NLTE plasmas created in the Livermore EBIT-I and EBIT-II. The x-ray emissions from the $5f \rightarrow 3d$ and $4f \rightarrow 3d$ of Ni-like to Kr-like gold ions have been recorded from monoenergetic electron beam plasmas having $E_{\rm beam} = 2.66$, 2.92, 3.53, and 4.54 keV, and the CSD of the beam plasmas has been inferred by fitting the collisionally excited line transitions and radiative recombination emissions with synthetic spectra. Yan *et al*. [34,35] theoretically studied the opacity of gold mixtures in the LTE by using the unresolved transition array model. Their results show that the Rosseland mean opacity of the mixtures will be increased when comparing with pure gold plasmas. Cheng *et al*. [36] simulated the opacities of hot and dense gold plasma in the LTE by the Monte Carlo method based on the UTA approximation. Yang *et al*. [37] experimentally verified that the Rosseland mean opacity of a mixture of gold and gadolinium is higher than that of the pure gold sample. Zeng *et al*. [38,39] theoretically calculated spectrally resolved opacities as well as Rosseland and Planck mean opacities of LTE gold plasmas by using a fully relativistic detailed level accounting (DLA) model and an average atom (AA) model, respectively. Gao *et al*. [40] calculated the electron-impact excitation of gold by using a semirelativistic distorted-wave method. Zhang [41], Bar-Shalom [27], and Gu [42] calculated the electron-impact excitation cross sections for the $3d \rightarrow 4f$ and $3d \rightarrow 5f$ processes by using DWS, HULLAC, and FAC codes, respectively. May [43] measured the cross sections for the $3d \rightarrow 4f$ and $3d \rightarrow 5f$ excitations of Ni-like to Ga-like gold ions in beam plasmas created in the Livermore EBIT-I. Yang *et al*. [44] calculated the electron-impact excitation energies and collision strengths for Ni-, Cu-, and Zn-like gold ions by using a fully RDW code REIE06. Meng *et al*. [45] studied the total dielectronic recombination (DR) rate coefficient from the ground and the first excited states of Co-like gold ions employing the relativistic distorted-wave approximation with configuration interaction. However, to our knowledge there are no systematic works on the degree of linear polarization for gold x-ray spectra in ICF relevant spectral regions. Therefore, in the present work, the cross sections for electron-impact excitation and capture to individual magnetic sublevels of Cu-like to Se-like gold ions are calculated by using the fully RDW method. And the degrees of linear polarization for the corresponding first two strongest $5f \rightarrow 3d$ transition lines are also calculated with the use of these magnetic sublevel cross sections. In Sec. II, the theoretical method is described. In Sec. III, the magnetic sublevel cross sections and the degrees of linear polarization of the corresponding lines are discussed. Finally, some brief conclusions of the present work are given in Sec. IV.

II. THEORETICAL METHOD

In the present work, a recently developed fully RDW code REIE06 [46–48] is used to calculate the electron-impact excitation cross sections, where the target state wave functions are generated with the use of the atomic structure package GRASP92 [49] based on the multiconfiguration Dirac-Fock (MCDF) method, and the continuum electron wave functions are produced by the component COWF of the RATIP package [50] by solving the coupled Dirac equation in which the exchange effect between the bound and continuum electrons are considered. In this method, the z axis is chosen along the motion of the incident electron, and then the z component of the incident electron orbital angular momentum is zero, namely, $m_{l_i} = 0$. In this case the electron-impact excitation cross section of the target ion from the initial state $\beta_i J_i M_i$ to the final state $\beta_f J_f M_f$ can be represented as [41,51]

$$\begin{aligned}\sigma_{\varepsilon_i}(\beta_i J_i M_i - \beta_f J_f M_f) = \frac{2\pi a_0^2}{k_{i^2}} \sum_{l_i, l_i', j_i, j_i', m_{s_i}, l_f, j_f, m_f} \sum_{J, J', M} (i)^{l_i - l_i'} [(2l_i + 1)(2l_i' + 1)]^{1/2} \exp\left[i\left(\delta_{\kappa_i} - \delta_{\kappa_i'}\right)\right] C\left(l_i \frac{1}{2} m_{l_i} m_{s_i}; j_i m_i\right) \\ \times C\left(l_i' \frac{1}{2} m_{l_i'} m_{s_i}; j_i' m_i\right) C(J_i j_i M_i m_i; J M) C(J_i j_i' M_i m_i; J' M) \\ \times C(J_f j_f M_f m_f; J M) C(J_f j_f M_f m_f; J' M) R(\gamma_i, \gamma_f) R(\gamma_i', \gamma_f'), \end{aligned} \tag{1}$$

where the subscripts i and f refer to the initial and final states, respectively; ε_i is the incident electron energy in Rydberg; a_0 is the Bohr radius; C's are Clebsch-Gordan coefficients; R's are the collision matrix elements; $\gamma_i = \varepsilon_i l_i j_i \beta_i J_i J M$ and $\gamma_f = \varepsilon_f l_f j_f \beta_f J_f J M$, where J and M are the quantum numbers corresponding to the total angular momentum of the impact system, target ion plus free electron, and its z component, respectively; β represents all additional quantum numbers required to specify the initial and final states of the target ion in addition to its total angular momentum J and z component M; m_{s_i}, l_i, j_i, m_{l_i}, and m_i are the spin, orbital angular momentum, total angular momentum, and its z-component quantum numbers, respectively, for the incident electron e_i; δ_{κ_i} is the phase factor for the continuum electron; κ is the relativistic quantum number, which is related to the orbital and total angular momentum l and j; k_i is the relativistic

wave number of the incident electron and is given by

$$k_i^2 = \varepsilon_i \left(1 + \frac{\alpha^2 \varepsilon_i}{4}\right), \tag{2}$$

and α is the fine-structure constant. It turns out that $R(\gamma_i, \gamma_f)$ are independent of M,

$$R(\gamma_i, \gamma_f) = \langle \Psi_{\gamma_f} | \sum_{p,q,p<q}^{N+1} (V_{\text{Coul}} + V_{\text{Breit}}) | \Psi_{\gamma_i} \rangle, \tag{3}$$

where Ψ_{γ_i} and Ψ_{γ_f} are the antisymmetric $N+1$ electron wave functions for the initial and final states of the impact systems, respectively; V_{Coul} is the Coulomb operator; and V_{Breit} is the Breit operator given by [49]

$$V_{\text{Breit}} = -\frac{\alpha_p \alpha_q}{r_{pq}} \cos(\omega_{pq} r_{pq}) + (\alpha_p \cdot \nabla_p)(\alpha_q \cdot \nabla_q) \frac{\cos(\omega_{pq} r_{pq}) - 1}{\omega_{pq}^2 r_{pq}}, \tag{4}$$

where α_p and α_q are the Dirac matrices, and ω_{pq} is the angular frequency of the exchanged virtual photon.

For initially randomly orientated target ions, the case of interest here, one can average over initial magnetic sublevels M_i of the target ion and obtain the cross section for excitation to a specific final magnetic sublevel M_f,

$$\sigma_{\varepsilon_i}(\beta_i J_i - \beta_f J_f M_f) = \frac{1}{2J_i + 1} \sum_{M_i} \sigma_{\varepsilon_i}(\beta_i J_i M_i - \beta_f J_f M_f). \tag{5}$$

The dielectronic recombination process can also form the excited state produced in the electron-impact excitation process above. Here, the capture cross section from the capture initial state i to the magnetic sublevels of capture final state f for unpolarized electrons is given by [51]

$$\sigma_{\varepsilon_i}^{\text{cap}}(\beta_i J_i M_i - \beta_f J_f M_f) = S^{\text{cap}}(\beta_i J_i M_i - \beta_f J_f M_f) \delta(\varepsilon_i - \varepsilon_{if}), \tag{6}$$

where

$$\begin{aligned} S^{\text{cap}}&(\beta_i J_i M_i - \beta_f J_f M_f) \\ &= \frac{2\pi a_0^2}{k_{i^2}} \sum_{l_i, l_i', j_i, j_i', m_{s_i}} (i)^{l_i - l_i'} [(2l_i + 1)(2l_i' + 1)]^{1/2} \\ &\times \exp\left[i\left(\delta_{\kappa_i} - \delta_{\kappa_i'}\right)\right] C\left(l_i \frac{1}{2} 0 m_{s_i}; j_i m_i\right) \\ &\times C\left(l_i' \frac{1}{2} 0 m_{s_i}; j_i' m_i\right) C(J_i j_i M_i m_i; J_f M_f) \\ &\times C(J_i j_i' M_i m_i; J_f M_f) R(\gamma_f, \gamma_i) R(\gamma_f', \gamma_i'). \end{aligned} \tag{7}$$

The degree of linear polarization of the radiation emitted without detecting the scattered electron is then defined by [52]

$$P = \frac{I_\parallel - I_\perp}{I_\parallel + I_\perp}, \tag{8}$$

where $I_\parallel$ and $I_\perp$ are the intensities of photons with electric vectors parallel and perpendicular to the electron beam direction, respectively.

The degree of linear polarization for radiation from the $J = 1$ to the $J = 0$ line is given by [52]

$$P = \frac{\sigma_0 - \sigma_1}{\sigma_0 + \sigma_1}. \tag{9}$$

If we assume that the electron-impact excitation process is the dominant mechanism for populating the upper magnetic sublevels, σ_0 and σ_1 are the electron-impact excitation cross sections from the ground state to the magnetic sublevels $M_f = 0$ and $M_f = 1$ of the excited state, respectively. However, if the dielectronic recombination process is the significant mechanism for populating the upper magnetic sublevels, σ_0 and σ_1 are the capture cross sections from the ground state to the magnetic sublevels $M_f = 0$ and $M_f = 1$ of the resonant doubly excited state, respectively.

Furthermore, the degree of linear polarization for radiation from the $J = 3/2$ to the $J = 1/2$ line is also given by [52]

$$P = \frac{3(\sigma_{1/2} - \sigma_{3/2})}{5\sigma_{1/2} + 3\sigma_{3/2}}. \tag{10}$$

Similarly, for the electron-impact excitation process, $\sigma_{1/2}$ and $\sigma_{3/2}$ are the electron-impact excitation cross sections from the ground state to the magnetic sublevels $M_f = 1/2$ and $M_f = 3/2$ of the excited state, respectively, while for the dielectronic recombination process, $\sigma_{1/2}$ and $\sigma_{3/2}$ are the capture cross sections from the ground state to the magnetic sublevels $M_f = 1/2$ and $M_f = 3/2$ of the resonant doubly excited state, respectively.

III. RESULTS AND DISCUSSIONS

A. Comparisons of transition energies and electron-impact excitation cross sections

In the calculations of wave functions and energy levels for the initial and final states, the contributions from the Breit interaction and quantum electrodynamics (QED) effect are taken into account. And in the calculations of the electron-impact excitation cross sections, the maximal partial $\kappa = 50$ is included in order to ensure convergence. In Table I, the calculated transition energies of some relatively strong $5f \rightarrow 3d$ lines for highly charged Cu-like to Se-like gold ions are shown along with other theoretical and experimental [23] values. It can be found that the present results are in very good agreement with these theoretical and experimental values within the experimental error. Taking the radiative line Cu-1 for example, the present transition energy is 3334.62 eV compared with the experimental measurement value 3334.7 ± 0.5 eV performed on the Livermore-EBIT [23] and the theoretical result 3334.48 eV given by HULLAC [23]. An agreement of $<0.05\%$ is quoted for the differences between HULLAC and the present calculated energies, but there are some lines of As-like and Se-like gold ions with differences $>0.1\%$. So the present single configuration model is accurate enough for these highly charged ions.

In order to further illustrate the accuracy of the present calculations, Fig. 1 displays the present calculated total and individual magnetic sublevel electron-impact excitation cross sections for the $3d_{3/2} \rightarrow 5f_{5/2}$ of Cu-like gold ions (labeled by Cu-3) along with the experimental results [43] and other theoretical results calculated with HULLAC [27], DWS [41],

TABLE I. Comparison of the transition energies (eV) of the $5f \rightarrow 3d$ process of highly charged Cu-like to Se-like gold ions between the present calculated results and other experimental and theoretical ones. Note that the closed subshell $4s^2$ has been omitted from the transitional initial and final states. Errors on the experimental photon energies in eV are given in parentheses, and "u" signifies an unidentified line.

Ion	Label	Transition	$J_i \rightarrow J_f$	Present	HULLAC [23]	Expt. 1 [53]	Expt. 2 [23]
Au^{50+}	Cu-1	$3d_{5/2}^{-1}4s5f_{7/2}$-$3d^{10}4s$	$\frac{3}{2}-\frac{1}{2}$	3334.62	3334.48	3335.3	3334.7(0.5)
	Cu-2	$3d_{5/2}^{-1}4s5f_{7/2}$-$3d^{10}4s$	$\frac{1}{2}-\frac{1}{2}$	3333.60	3333.49	3332.7	3333.2(0.5)
	Cu-3	$3d_{3/2}^{-1}4s5f_{5/2}$-$3d^{10}4s$	$\frac{3}{2}-\frac{1}{2}$	3418.71	3419.07		3420.8(0.6)
	Cu-4	$3d_{3/2}^{-1}4s5f_{5/2}$-$3d^{10}4s$	$\frac{1}{2}-\frac{1}{2}$	3418.95	3419.45		3426.2(0.5)
Au^{49+}	Zn-1	$3d_{5/2}^{-1}5f_{7/2}$-$3d^{10}$	$1-0$	3300.06	3302.42	3301.1	3296.6(0.5)
	Zn-2	$3d_{3/2}^{-1}5f_{5/2}$-$3d^{10}$	$1-0$	3384.34	3387.14		3382.7(0.5)
Au^{48+}	Ga-1	$3d_{5/2}^{-1}4p_{1/2}5f_{7/2}$-$3d^{10}4p_{1/2}$	$\frac{3}{2}-\frac{1}{2}$	3264.58	3265.88		3259.9(0.5)
	Ga-2	$3d_{5/2}^{-1}4p_{1/2}5f_{7/2}$-$3d^{10}4p_{1/2}$	$\frac{1}{2}-\frac{1}{2}$	3264.77	3266.31		u
	Ga-3	$3d_{3/2}^{-1}4p_{1/2}5f_{5/2}$-$3d^{10}4p_{1/2}$	$\frac{3}{2}-\frac{1}{2}$	3349.93	3351.70	3349.2	3348.3(0.5)
	Ga-4	$3d_{3/2}^{-1}4p_{1/2}5f_{5/2}$-$3d^{10}4p_{1/2}$	$\frac{1}{2}-\frac{1}{2}$	3348.35	3350.34	3345.3	3345.3(0.6)
Au^{47+}	Ge-1	$3d_{5/2}^{-1}4p_{1/2}^2 5f_{7/2}$-$3d^{10}4p_{1/2}^2$	$1-0$	3229.38	3230.99		3226.5(0.5)
	Ge-2	$3d_{3/2}^{-1}4p_{1/2}^2 5f_{5/2}$-$3d^{10}4p_{1/2}^2$	$1-0$	3314.19	3316.56	3315.6	3312.2(0.6)
Au^{46+}	As-1	$3d_{5/2}^{-1}4p_{1/2}4p_{3/2}^2 5f_{7/2}$-$3d^{10}4p_{1/2}4p_{3/2}^2$	$\frac{3}{2}-\frac{1}{2}$	3200.82			
	As-2	$3d_{5/2}^{-1}4p_{1/2}^2 4p_{3/2}5f_{7/2}$-$3d^{10}4p_{1/2}^2 4p_{3/2}$	$\frac{1}{2}-\frac{3}{2}$	3197.49	3200.96		3191.1(0.7)
	As-3	$3d_{5/2}^{-1}4p_{1/2}^2 4p_{3/2}5f_{7/2}$-$3d^{10}4p_{1/2}^2 4p_{3/2}$	$\frac{3}{2}-\frac{3}{2}$	3191.92	3200.33		u
	As-4	$3d_{5/2}^{-1}4p_{1/2}^2 4p_{3/2}5f_{7/2}$-$3d^{10}4p_{1/2}^2 4p_{3/2}$	$\frac{5}{2}-\frac{3}{2}$	3198.35	3201.71		3194.1(0.5)
	As-5	$3d_{3/2}^{-1}4p_{1/2}4p_{3/2}^2 5f_{5/2}$-$3d^{10}4p_{1/2}4p_{3/2}^2$	$\frac{3}{2}-\frac{1}{2}$	3285.68			
	As-6	$3d_{3/2}^{-1}4p_{1/2}^2 4p_{3/2}5f_{5/2}$-$3d^{10}4p_{1/2}^2 4p_{3/2}$	$\frac{1}{2}-\frac{3}{2}$	3282.65	3286.75	3284.0	3283.7(0.6)
	As-7	$3d_{3/2}^{-1}4p_{1/2}^2 4p_{3/2}5f_{5/2}$-$3d^{10}4p_{1/2}^2 4p_{3/2}$	$\frac{3}{2}-\frac{3}{2}$	3281.26	3285.36		3273.7(0.5)
	As-8	$3d_{3/2}^{-1}4p_{1/2}^2 4p_{3/2}5f_{5/2}$-$3d^{10}4p_{1/2}^2 4p_{3/2}$	$\frac{5}{2}-\frac{3}{2}$	3282.31	3286.23		3276.8(0.6)
Au^{45+}	Se-1	$3d_{5/2}^{-1}4p_{1/2}^2 4p_{3/2}^2 5f_{7/2}$-$3d^{10}4p_{1/2}^2 4p_{3/2}^2$	$1-0$	3165.71	3167.14		u
	Se-2	$3d_{5/2}^{-1}4p_{1/2}^2 4p_{3/2}^2 5f_{7/2}$-$3d^{10}4p_{1/2}^2 4p_{3/2}^2$	$1-2$	3164.54	3167.27		3164.2(0.6)
	Se-3	$3d_{5/2}^{-1}4p_{1/2}^2 4p_{3/2}^2 5f_{7/2}$-$3d^{10}4p_{1/2}^2 4p_{3/2}^2$	$2-2$	3165.51	3167.84		3179.8(0.7)
	Se-4	$3d_{3/2}^{-1}4p_{1/2}^2 4p_{3/2}^2 5f_{5/2}$-$3d^{10}4p_{1/2}^2 4p_{3/2}^2$	$1-0$	3250.01	3252.03		u
	Se-5	$3d_{3/2}^{-1}4p_{1/2}^2 4p_{3/2}^2 5f_{5/2}$-$3d^{10}4p_{1/2}^2 4p_{3/2}^2$	$1-2$	3249.44	3252.77		3245.8(0.5)
	Se-6	$3d_{3/2}^{-1}4p_{1/2}^2 4p_{3/2}^2 5f_{5/2}$-$3d^{10}4p_{1/2}^2 4p_{3/2}^2$	$2-2$	3249.41	3252.97		u

as well as FAC [42]. FAC and DWS show the cross sections for excitation to the individual magnetic sublevels. Here, the magnetic sublevel cross sections for excitation from the magnetic sublevels $M_i = \pm 1/2$ of the ground state to the magnetic sublevels $M_f = \mp 3/2$ of the excited state are very small (less than almost four orders) when comparing with other magnetic sublevel cross sections for excitation from the magnetic sublevels $M_i = \pm 1/2$ of the ground state to the magnetic sublevels $M_f = \pm 3/2$, $M_f = \pm 1/2$, and $M_f = \mp 1/2$ of the excited states, so they are not plotted in the figure. It can be found that the agreement of individual magnetic sublevel cross sections is relatively good among the different theoretical results, and the maximal difference between the present and other results is within 5%. For the total cross sections, the present results are also in good agreement with other theoretical results. However, all the theoretical cross sections included in Fig. 1 are slightly larger than the experimental results.

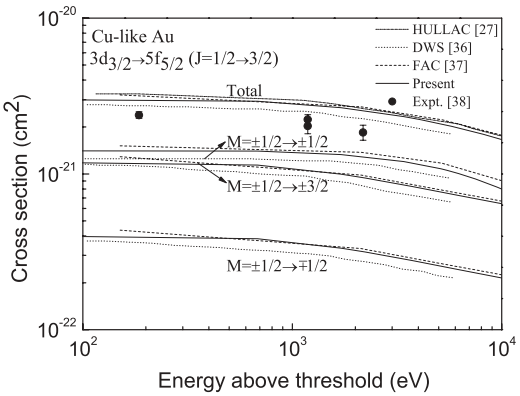

FIG. 1. Comparison of total and magnetic sublevel electron-impact excitation cross sections for the process $3d_{3/2} \rightarrow 5f_{5/2}$ of Cu-like gold ions between the present calculated results and other experimental and theoretical results from FAC, HULLAC, and DWS.

B. Electron-impact excitation cross sections

On the basis of the above comparison of cross sections, Fig. 2 presents the total and individual magnetic sublevel electron-impact excitation cross sections for the $3d_{3/2} \rightarrow 5f_{5/2}$ and $3d_{5/2} \rightarrow 5f_{7/2}$ processes of Cu-like to Se-like gold

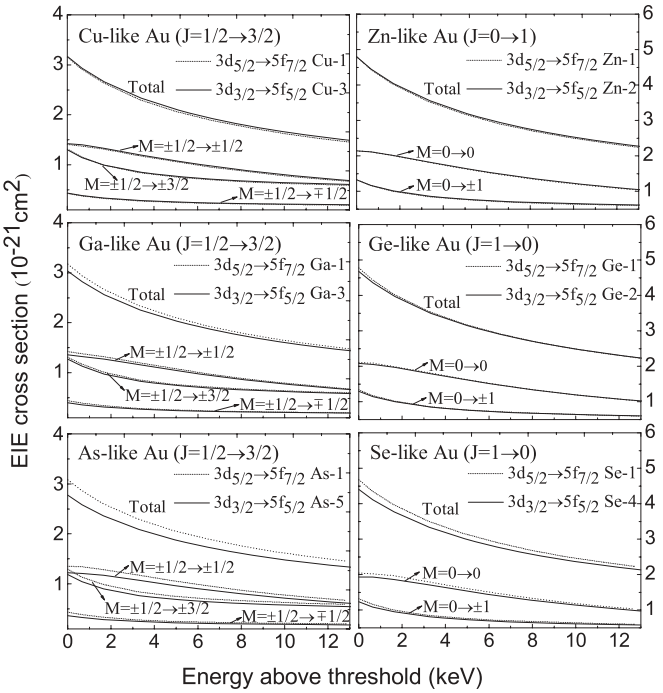

FIG. 2. The total and magnetic sublevel cross sections for Cu-like to Se-like gold ions as functions of incident electron energy. The solid lines represent the values for the excitation from $3d_{3/2}$ to $5f_{5/2}$, and the dashed lines represent the results from $3d_{5/2}$ to $5f_{7/2}$.

ions as functions of incident electron energy. It is found that the total cross sections decrease monotonically as incident electron energy increases; they decrease rapidly near the threshold energy but slowly within a higher energy region. For Cu-, Ga-, and As-like gold ions, the cross sections for excitation to magnetic sublevels $M_f = \pm 1/2$ are larger than sublevels $M_f = \pm 3/2$ and $M_f = \mp 1/2$, the cross sections for excitation to magnetic sublevels $M_f = \mp 1/2$ are the smallest ones at any given incident electron energy. As for Zn-, Ge-, and Se-like gold ions, the cross sections for excitation to magnetic sublevel $M_f = 0$ are significantly larger than $M_f = \pm 1$. For all of the gold ions, the total and individual magnetic sublevel cross sections for the excitation $3d_{3/2} \rightarrow 5f_{5/2}$ are the same as those for excitation $3d_{3/2} \rightarrow 5f_{5/2}$. The total and individual magnetic sublevel cross sections for Cu-like gold ions are nearly uniform with those of Ga-like and As-like gold ions. Similarly, the total and individual magnetic sublevel cross sections for Zn-like gold ions are also approximately the same as those for Ge-like and Se-like gold ions.

C. Resonant energies and capture cross sections

Dielectronic recombination of Ni-like to As-like gold ions can also form the same excited states formed in electron-impact excitation of Cu-like to Se-like gold ions. In Table II, labels of the capture initial states and final states (doubly excited states) for the first two strongest processes of the six different charged gold ions from Cu-like to Se-like are presented along with the corresponding dielectronic recombination resonant energies. It can be found that for all relevant gold ions the capture final states are the same as the excited final states (see Table I) formed in the electron-impact excitation process, respectively. For all the gold ions, the dielectronic recombination resonant energies of $3d_{3/2} \rightarrow 5f_{5/2}$ are greater than those for $3d_{5/2} \rightarrow 5f_{7/2}$, and the absolute differences between the two kinds of energy are roughly 84 eV. Also, the relative values decrease steadily from 17.7% to 9.6% for Cu-like to Se-like gold ions.

Total and magnetic sublevel capture cross sections (CCS) for Cu-like to Se-like gold ions are presented in Table III, in which $M_i \rightarrow M_f$ represents capture cross sections from the magnetic sublevel M_i of the capture initial state to the magnetic sublevel M_f of the capture final state. It can be found that some specific magnetic capture cross sections are equal to zero, such as $\sigma_{M=0\rightarrow\pm 3/2}$ for Cu-, Ga-, and As-like gold ions, $\sigma_{M=\pm 1/2\rightarrow\mp 1}$ for Zn- and Ge-like gold ions, as well as $\sigma_{M=\pm 1/2\rightarrow\mp 1}$, $\sigma_{M=\pm 3/2\rightarrow 0}$, and $\sigma_{M=\pm 3/2\rightarrow\mp 1}$ for Se-like gold ions, which have a common characteristic, that is, $\Delta M > 1$. Compared with electron-impact excitation cross sections, capture cross sections are larger than those at all given incident

TABLE II. The dielectronic recombination resonant energies (eV) for the first two strongest capture processes of Cu-like to Se-like gold ions, where the capture final states are the same as the excited states of the electron-impact excitation process of all gold ions, respectively.

Ion	Label	$J_i \rightarrow J_f$	Initial state	Final state	Resonant energy
Au^{50+}	Cu-1	$0 \rightarrow \frac{3}{2}$	$3d^{10}$	$3d_{5/2}^{-1}4s5f_{7/2}$	389.74
	Cu-3	$0 \rightarrow \frac{3}{2}$	$3d^{10}$	$3d_{3/2}^{-1}4s5f_{5/2}$	473.82
Au^{49+}	Zn-1	$\frac{1}{2} \rightarrow 1$	$3d^{10}4s$	$3d_{5/2}^{-1}4s^25f_{7/2}$	427.45
	Zn-2	$\frac{1}{2} \rightarrow 1$	$3d^{10}4s$	$3d_{3/2}^{-1}4s^25f_{5/2}$	511.73
Au^{48+}	Ga-1	$0 \rightarrow \frac{3}{2}$	$3d^{10}4s^2$	$3d_{5/2}^{-1}4s^24p_{1/2}5f_{7/2}$	556.88
	Ga-3	$0 \rightarrow \frac{3}{2}$	$3d^{10}4s^2$	$3d_{3/2}^{-1}4s^24p_{1/2}5f_{5/2}$	642.23
Au^{47+}	Ge-1	$\frac{1}{2} \rightarrow 1$	$3d^{10}4s^24p_{1/2}$	$3d_{5/2}^{-1}4s^24p_{1/2}^25f_{7/2}$	589.27
	Ge-2	$\frac{1}{2} \rightarrow 1$	$3d^{10}4s^24p_{1/2}$	$3d_{3/2}^{-1}4s^24p_{1/2}^25f_{5/2}$	674.08
Au^{46+}	As-1	$0 \rightarrow \frac{3}{2}$	$3d^{10}4s^24p_{1/2}^2$	$3d_{5/2}^{-1}4s^24p_{1/2}4p_{3/2}^25f_{7/2}$	897.75
	As-5	$0 \rightarrow \frac{3}{2}$	$3d^{10}4s^24p_{1/2}^2$	$3d_{3/2}^{-1}4s^24p_{1/2}4p_{3/2}^25f_{5/2}$	982.62
Au^{45+}	Se-1	$\frac{3}{2} \rightarrow 1$	$3d^{10}4s^24p_{1/2}^24p_{3/2}$	$3d_{5/2}^{-1}4s^24p_{1/2}^24p_{3/2}^25f_{7/2}$	791.75
	Se-4	$\frac{3}{2} \rightarrow 1$	$3d^{10}4s^24p_{1/2}^24p_{3/2}$	$3d_{3/2}^{-1}4s^24p_{1/2}^24p_{3/2}^25f_{5/2}$	876.05

TABLE III. Total and magnetic sublevel CCS (cm^2) for Cu-like to Se-like gold ions, $M_i \to M_f$ represents the capture cross section from the magnetic sublevel M_i of the capture initial state to the magnetic sublevel M_f of the capture final state.

Ion	Label	$J_i \to J_f$	M-dependent CCS						Total CCS
Au^{50+}			$0 \to \pm\frac{1}{2}$	$0 \to \pm\frac{3}{2}$					
	Cu-1	$0 \to \frac{3}{2}$	2.48×10^{-19}	0					4.96×10^{-19}
	Cu-3	$0 \to \frac{3}{2}$	2.84×10^{-19}	0					5.68×10^{-19}
Au^{49+}			$\pm\frac{1}{2} \to 0$	$\pm\frac{1}{2} \to \mp 1$	$\pm\frac{1}{2} \to \pm 1$				
	Zn-1	$\frac{1}{2} \to 1$	1.29×10^{-19}	0	3.22×10^{-21}				1.32×10^{-19}
	Zn-2	$\frac{1}{2} \to 1$	1.26×10^{-19}	0	1.38×10^{-20}				1.40×10^{-19}
Au^{48+}			$0 \to \pm\frac{1}{2}$	$0 \to \pm\frac{3}{2}$					
	Ga-1	$0 \to \frac{3}{2}$	1.49×10^{-20}	0					2.98×10^{-20}
	Ga-3	$0 \to \frac{3}{2}$	7.46×10^{-21}	0					1.49×10^{-20}
Au^{47+}			$\pm\frac{1}{2} \to 0$	$\pm\frac{1}{2} \to \mp 1$	$\pm\frac{1}{2} \to \pm 1$				
	Ge-1	$\frac{1}{2} \to 1$	2.99×10^{-20}	0	1.17×10^{-20}				4.16×10^{-20}
	Ge-2	$\frac{1}{2} \to 1$	3.15×10^{-20}	0	2.02×10^{-20}				5.17×10^{-20}
Au^{46+}			$0 \to \pm\frac{1}{2}$	$0 \to \pm\frac{3}{2}$					
	As-1	$0 \to \frac{3}{2}$	3.72×10^{-24}	0					7.44×10^{-24}
	As-5	$0 \to \frac{3}{2}$	1.63×10^{-25}	0					3.26×10^{-25}
Au^{45+}			$\pm\frac{1}{2} \to 0$	$\pm\frac{1}{2} \to \mp 1$	$\pm\frac{1}{2} \to \pm 1$	$\pm\frac{3}{2} \to 0$	$\pm\frac{3}{2} \to \mp 1$	$\pm\frac{3}{2} \to \pm 1$	
	Se-1	$\frac{3}{2} \to 1$	1.04×10^{-21}	0	1.77×10^{-21}	0	0	6.54×10^{-21}	4.68×10^{-21}
	Se-4	$\frac{3}{2} \to 1$	6.47×10^{-22}	0	1.53×10^{-21}	0	0	5.39×10^{-21}	3.78×10^{-21}

electron energies for Cu-like to Ge-like gold ions, however, there is an exception for As-like gold ions around the threshold energies and for Se-like gold ions at all given incident electron energies.

D. Degrees of polarization for electron-impact excitation and dielectronic recombination processes

Figure 3 displays the degrees of linear polarization of the corresponding lines following the electron-impact excitation process as functions of incident electron energy in threshold units. For all the gold ions, the degrees of linear polarization for the excitation $3d_{3/2} \to 5f_{5/2}$ are almost same as the ones for the excitation $3d_{5/2} \to 5f_{7/2}$. The degrees of linear polarization increase sharply with an increase of incident electron energy before starting to decrease at the higher energy region, and reach their respectively corresponding maximum at roughly two times the threshold energy. The same pattern had been found in the intermediate coupling calculations for heliumlike Fe ions by Inal *et al.* [54] and in the distorted-wave calculations for several heliumlike ions by Reed *et al.* [55]. For Cu-like gold ions the degree of linear polarization changes in the range of 0.1–0.2 within five times the threshold energy, however, the degree of linear polarization for Zn-like gold ions changes among the range of 0.20–0.36 within the same energy range. Therefore, the degrees of linear polarization for Cu-like gold ions are larger than the ones for Zn-like gold ions at any given incident electron energies. It can be found that the cross sections for Ga-like and As-like gold ions are very similar with Cu-like gold ions, and the situations of Ge-like and Se-like gold ions are almost same as Zn-like gold ions.

In Table IV, we display the degrees of linear polarization for the same radiative lines but formed by the dielectronic recombination process. The degrees of linear polarization of these radiative lines formed by dielectronic recombination are quite different for different gold ions. For Cu-, Ga- and As-like gold ions, because the cross sections for capturing the individual magnetic sublevel $M_f = 3/2$ of the resonant doubly

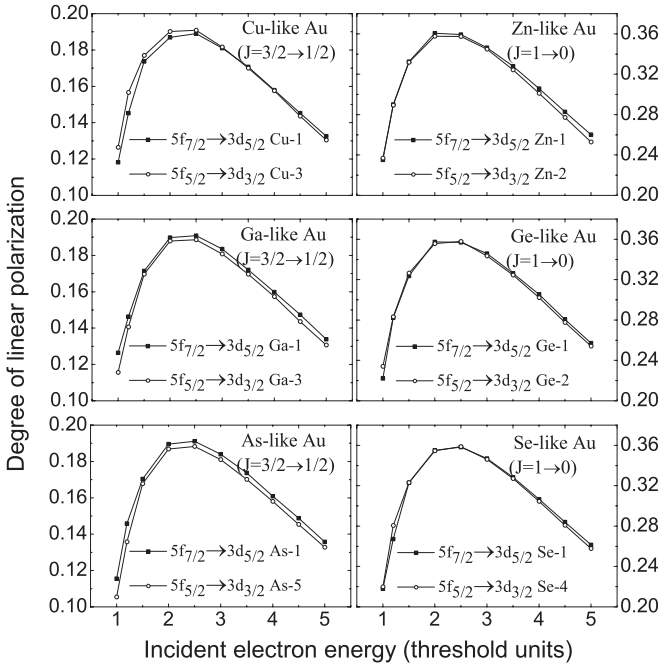

FIG. 3. The degrees of linear polarization for Cu-like to Se-like gold ions as functions of incident electron energy. The circles represent the values for the excitation from $3d_{3/2}$ to $5f_{5/2}$, and the dark squares represent the results for excitation to $5f_{7/2}$ from $3d_{5/2}$.

TABLE IV. Linear degrees of polarization of the corresponding radiations $5f_{7/2} \rightarrow 3d_{5/2}$ and $5f_{5/2} \rightarrow 3d_{3/2}$ following the dielectronic recombination process of Cu-like to Se-like gold ions.

Ion	Label	Transition	Polarization
Au^{50+}	Cu-1	$5f_{7/2} \rightarrow 3d_{5/2}$	0.6
	Cu-3	$5f_{5/2} \rightarrow 3d_{3/2}$	0.6
Au^{49+}	Zn-1	$5f_{7/2} \rightarrow 3d_{5/2}$	0.98
	Zn-2	$5f_{5/2} \rightarrow 3d_{3/2}$	0.90
Au^{48+}	Ga-1	$5f_{7/2} \rightarrow 3d_{5/2}$	0.6
	Ga-3	$5f_{5/2} \rightarrow 3d_{3/2}$	0.6
Au^{47+}	Ge-1	$5f_{7/2} \rightarrow 3d_{5/2}$	0.67
	Ge-2	$5f_{5/2} \rightarrow 3d_{3/2}$	0.52
Au^{46+}	As-1	$5f_{7/2} \rightarrow 3d_{5/2}$	0.6
	As-5	$5f_{5/2} \rightarrow 3d_{3/2}$	0.6
Au^{45+}	Se-1	$5f_{7/2} \rightarrow 3d_{5/2}$	−0.59
	Se-4	$5f_{5/2} \rightarrow 3d_{3/2}$	−0.68

excited states from the respectively corresponding ground states are equal to zero, the degrees of linear polarization of the resulting lines are equal to 0.6 by using Eq. (10). However, for other gold ions the situations of linear polarization are quite different. For example, for Zn-like gold ions the degrees of linear polarization are equal to 0.98 for the radiative line $5f_{7/2} \rightarrow 3d_{5/2}$ (labeled by Zn-1) and 0.90 for the line $5f_{5/2} \rightarrow 3d_{3/2}$ (labeled by Zn-2); for Ge-like gold ions the degrees of linear polarization are 0.67 and 0.52 for the radiative lines Ge-1 and Ge-2, as well as the degrees of linear polarization prove to be −0.59 and −0.68 for the radiative lines Se-1 and Se-4 of Se-like gold ions, respectively. It is found that the degrees of linear polarization for the line $5f_{7/2} \rightarrow 3d_{5/2}$ are greater than those for the line $5f_{5/2} \rightarrow 3d_{3/2}$ of Zn-, Ge-, and Se-like gold ions. It is also found that the degrees of linear polarization of these lines formed by electron-impact excitation are very different from those for the same radiative lines but formed by the dielectronic recombination process. Therefore, we can use these degrees of linear polarization to distinguish and identify the formation mechanism of the corresponding radiative lines. Furthermore, the specific plasma conditions can also be assessed by measuring these linear polarizations of the corresponding spectral lines. For example, electron-impact excitation would dominate in hot and dense plasmas and the dielectronic recombination process would dominate in low-density plasmas that are cooled and recombining by capturing the continuum electrons. Admittedly, besides the formation mechanism of spectral lines, radiative cascade effect and metastable states can also greatly affect the linear polarizations of the corresponding lines in some cases. However, according to our calculations, the excitation and capture cross sections to the relevant cascading levels are much smaller than those to the upper level of interest, less than almost four orders, and the excitation and capture cross sections from a metastable state into the upper levels are also very small compared with the cross sections of interest. So the contributions of the cascade effect and the metastable states should be small.

IV. CONCLUSION

In the present paper, cross sections for electron-impact excitation and capture to individual magnetic sublevels of Cu-like to Se-like gold ions have been calculated by using a fully relativistic distorted-wave method. Furthermore, these cross sections are further employed in calculating the degrees of linear polarization of the corresponding first two strongest $5f \rightarrow 3d$ radiations. We compare the linear polarizations of these lines formed by electron-impact excitation with those of the same lines but formed by the dielectronic recombination process. It is found that for the electron-impact excitation process the degrees of linear polarization increase sharply before starting to decrease at higher energy regions and they reach the respective maximum at about two times that of the threshold energies. The degrees of linear polarization change in a range of 0.1–0.2 within five times that of the threshold energies for Cu-, Ga-, and As-like gold ions, while for Zn-, Ge-, and Se-like gold ions the degrees of linear polarization change among the range of 0.20–0.36 within the same energy range. As for the dielectronic recombination process, the degrees of linear polarization change in a very large range with different gold ions. For Cu-, Ga-, and As-like gold ions the degrees of linear polarization are equal to 0.6. And for Zn-, Ge-, and Se-like gold ions, the degrees of linear polarization are equal to 0.98, 0.67, and −0.59 for the radiative line $5f_{7/2} \rightarrow 3d_{5/2}$ as well as 0.90, 0.52, and −0.68 for the line $5f_{5/2} \rightarrow 3d_{3/2}$, respectively. It is also found that the differences of linear polarization between both electron-impact excitation and dielectronic recombination are very large. So we can use these degrees of linear polarization to diagnose the formation mechanism of these corresponding lines. Furthermore, the specific plasma conditions could further be assessed by measuring the linear polarizations of corresponding spectral lines. For example, electron-impact excitation would dominate in hot and dense plasmas and the dielectronic recombination process would dominate in low-density plasmas that are cooled and recombining by capturing the continuum electrons.

ACKNOWLEDGMENTS

This work has been supported by the National Natural Science Foundation of China (Grants No. 11274254, No. 10964010, No. 10876028, and No. 10847007), the Specialized Research Fund for the Doctoral Program of Higher Education of China (Grant No. 20070736001), and the Foundation of Center of Theoretical Nuclear Physics of National Laboratory of Heavy Ion Accelerator of Lanzhou).

[1] C. De Michelis and M. Mattioli, Rep. Prog. Phys. **47**, 1233 (1984).

[2] J. E. Rice, J. L. Terry, K. B. Fournier, M. A. Grarf, M. Finkenthal, M. J. May, E. S. Marmar, W. H. Goldstein, and A. E. Hubbard, J. Phys. B **29**, 2191 (1996).

[3] P. Buratti, E. Barbato, G. Bracco, S. Cirant, F. Crisanti, G. Granucci, A. A. Tuccillo, V. Zanza, M. Zerbini, L. Acitelli, F. Alladio, B. Angelini, M. L. Apicella, G. Apruzzese, L. Bertalot, A. Bertocchi, M. Borra, A. Bruschi, G. Buceti, A. Cardinali, C. Centioli, R. Cesario, C. Cianfarani, S. Ciattaglia,

V. Cocilovo, R. De Angelis, F. De Marco, B. Esposito, D. Frigione, L. Gabellieri, G. Gatti, E. Giovannozzi, C. Gourlan, M. Grolli, A. Imparato, H. Kroegler, M. Leigheb, L. Lovisetto, G. Maddaluno, G. Maffia, M. Marinucci, G. Mazzitelli, P. Micozzi, F. Mirizzi, S. Nowak, F. P. Orsitto, D. Pacella, L. Panaccione, M. Panella, V. Pericoli Ridolfini, L. Pieroni, S. Podda, G. B. Righetti, F. Romanelli, F. Santini, M. Sassi, S. E. Segre, A. Simonetto, C. Sozzia, S. Sternini, O. Tudisco, V. Vitale, G. Vlad, and F. Zonca, Phys. Rev. Lett. **82**, 560 (1999).

[4] R. Beier, C. Bachmann, and R. Burhenn, J. Phys. D **14**, 643 (1981).

[5] J. C. Raymond and N. C. Brickhouse, Astrophys. Space Sci. **237**, 321 (1996).

[6] K. L. Wong, P. T. Springer, J. H. Hammer, C. A. Iglesias, A. L. Osterheld, M. E. Foord, H. C. Bruns, and J. A. Emig, Phys. Rev. Lett. **80**, 2334 (1998).

[7] A. L. Velikovich, J. Davis, V. I. Oreshkin, J. P. Apruzese, R. Q. Clark, J. W. Thornhill, and L. I. Rudakov, Phys. Plasmas **8**, 4509 (2001).

[8] A. S. Shlyaptseva, S. B. Hansen, V. L. Kantsyrev, B. S. Bauer, D. A. Fedin, N. Ouart, S. A. Kazantsev, A. G. Petrashen, and U. I. Safronova, Rev. Sci. Instrum. **72**, 1241 (2001).

[9] A. S. Shlyaptseva, V. L. Kantsyrev, N. Ouart, D. Fedin, S. Hamasha, and S. Hansen, Proc. SPIE **5196**, 16 (2003).

[10] E. Haug, Sol. Phys. **61**, 129 (1979).

[11] E. Haug, Sol. Phys. **71**, 77 (1981).

[12] H. R. Griem, Phys. Fluids B **4**, 2346 (1992).

[13] J. C. Kieffer, J. P. Matte, M. Chaker, Y. Beaudoin, C. Y. Chien, S. Coe, G. Mourou, J. Dubau, and M. K. Inal, Phys. Rev. E **48**, 4648 (1993).

[14] C. Y. Côté, J. C. Kieffer, and O. Peyrusse, Phys. Rev. E **56**, 992 (1997).

[15] M. Fajardo, P. Audebert, P. Renaudin, H. Yashiro, R. Shepherd, J.-C. Gauthier, and C. Chenais-Popovics, Phys. Rev. Lett. **86**, 1231 (2001).

[16] Lindl J, Phys. Plasmas **2**, 3933 (1995).

[17] S. Kiyokawa, T. Yabe, N. Miyanaga, K. Okada, H. Hasegawa, T. Mochizuki, T. Yamanaka, C. Yamanaka, and T. Kagawa, Phys. Rev. Lett. **54**, 1999 (1985).

[18] C. Bauche-Arnoult, E. Luc-Koenig, J.-F. Wyart, J.-P. Geindre, P. Audebert, P. Monier, J.-C. Gauthier, and C. Chenais-Popovics, Phys. Rev. A **33**, 791 (1986).

[19] K. Honda, K. Mima, and F. Koike, Phys. Rev. E **55**, 4594 (1997).

[20] J. Y. Zhang, G. H. Yang, B. H. Zhang, X. D. Yang, Y. Q. Zhou, A. L. Lei, H. J. Liu, J. Li, J. M. Yang, and Y. N. Ding, High Power Laser and Particle Beams **13**, 186 (2001).

[21] J. Y. Zhang, G. H. Yang, Z. J. Zheng, J. M. Yang, Y. N. Ding, W. H. Zhang, and J. Li, High Power Laser and Particle Beams **15**, 981 (2003).

[22] Y. G. Yi, Z. J. Zheng, Y. J. Tang, and Z. H. Zhu, Nucl. Fusion Plasma Phys.**23**, 215 (2003).

[23] M. J. May, K. B. Fournier, P. Beiersdorfer, H. Chen, and K. L. Wong, Phys. Rev. E **68**, 036402 (2003).

[24] E. Träbert, P. Beiersdorfer, K. B. Fournier, S. B. Utter, and K. L. Wong, Can. J. Phys. **79**, 153162 (2001).

[25] J. L. Zeng, G. Zhao, and J. M. Yuan, Chin. Phys. Lett. **22**, 1972 (2005).

[26] M. E. Foord, S. H. Glenzer, R. S. Thoe, K. L. Wong, K. B. Fournier, B. G. Wilson, and P. T. Springer, Phys. Rev. Lett. **85**, 992 (2000).

[27] A. Bar-Shalom, M. Klapisch, and J. Oreg, J. Quant. Spectrosc. Radiat. Transf. **71**, 169 (2001).

[28] S. H. Glenzer, K. B. Fournier, B. G. Wilson, R. W. Lee, and L. J. Suter, Phys. Rev. Lett. **87**, 045002 (2001).

[29] B. G. Wilson, J. R. Albritton, and D. A. Liberman, in *Radiative Properties of Hot Dense Matter*, edited by W. Goldstein, C. Hooper, J. Gauthier, J. Seely, and R. Lee (World Scientific, Singapore, 1991).

[30] K. L. Wong, M. J. May, P. Beiersdorfer, B. Wilson, G. V. Brown, P. Springer, P. A. Neill, and L. Harris, Phys. Rev. Lett. **90**, 235001 (2003).

[31] O. Peyrusse, C. Bauche-Arnoult, and J. Bauche, J. Phys. B **38**, L137 (2005).

[32] R. F. Heeter, S. B. Hansen, K. B. Fournier, M. E. Foord, D. H. Froula, A. J. Mackinnon, M. J. May, M. B. Schneider, and B. K. F. Young, Phys. Rev. Lett. **99**, 195001 (2007).

[33] M. J. May, S. B. Hansen, J. Scofield, M. Schneider, K. Wong, and P. Beiersdorfer, Phys. Rev. E **84**, 046402 (2011).

[34] J. Yan and Y. B. Qiu, Phys. Rev. E **64**, 056401 (2001).

[35] J. Yan and Z. Q. Wu, Phys. Rev. E **65**, 066401 (2002).

[36] X. L. Cheng, L. Yang, H. Zhang, and X. D. Yang, Chin. Phys. Lett. **19**, 931 (2002).

[37] J. M. Yang, Y. Xu, Y. N. Ding, Y. K. Ding, S. E. Jiang, Z. J. Zheng, and W. Y. Miao, Chin. Phys. Lett. **20**, 256 (2003).

[38] J. L. Zeng and J. M. Yuan, Phys. Rev. E **76**, 026401 (2007).

[39] J. L. Zeng, J. Phys. B **41**, 125702 (2008).

[40] J. F. Gao, W. N. Pang, H. Gao, and R. C. Shang, Chin. Phys. Lett. **16**, 643 (1999).

[41] H. L. Zhang, D. H. Sampson, and R. E. H. Clark, Phys. Rev. A **41**, 198 (1990).

[42] *Proceedings of the 14th APS Topical Conference on Atomic Processes in Plasmas*, edited by M. F. Gu, J. S. Cohen, S. Mazevet, and D. P. Kilcrease, AIP Conf. Proc. No. 730 (AIP, New York, 2004), p. 127.

[43] M. J. May, P. Beiersdorfer, N. Jordan, J. H. Scofield, K. J. Reed, S. B. Hansen, K. B. Fournier, M. F. Gu, G. V. Brown, F. S. Porter, R. Kelley, C. A. Kilbourne, and K. R. Boyce, Nucl. Instrum. Methods Phys. Res. B **235**, 231 (2005).

[44] N. X. Yang, C. Z. Dong, and J. Jiang, Chin. Phys. Lett. **26**, 053401 (2009).

[45] F. C. Meng, C. Y. Chen, X. H. Shi, Y. S. Wang, Y. M. Zou, and M. F. Gu, J. Phys. B **40**, 4269 (2007).

[46] Z. W. Wu, J. Jiang, and C. Z. Dong, Phys. Rev. A **84**, 032713 (2011).

[47] J. Jiang, C. Z. Dong, L. Y. Xie, and J. G. Wang, Phys. Rev. A **78**, 022709 (2008).

[48] J. Jiang, C. Z. Dong, L. Y. Xie, J. G. Wang, J. Yan, and S. Fritzsche, Chin. Phys. Lett. **24**, 691 (2007).

[49] F. A. Parpia, C. F. Fischer, and I. P. Grant, Comput. Phys. Commun. **94**, 249 (1996).

[50] S. Fritzsche, H. Aksela, C. Z. Dong, S. Heinäsmäki, and J. E. Sienkiewicz, Nucl. Instrum. Methods Phys. Res. B **205**, 93 (2003).

[51] H. L. Zhang and D. H. Sampson, Phys. Rev. A **66**, 042704 (2002).

[52] I. C. Percival and M. J. Seaton, Philos. Trans. R. Soc. London, Ser. A **251**, 113 (1958).

[53] J. M. Yang *et al*. (unpublished).

[54] M. K. Inal and J. Dubau, J. Phys. B **20**, 4221 (1987).

[55] K. J. Reed and M. H. Chen, Phys. Rev. A **48**, 3644 (1993).